Available online at www.sciencedirect.com
ScienceDirect
Journal of the European Ceramic Society 29 (2009) 581–586
www.elsevier.com/locate/jeurceramsoc

Sintering behavior of periclase–doloma refractory mixes

A.G. Tomba Martinez [a,*], M.A. Camerucci [a], A.L. Cavalieri [a], L. Martorello [b], P.G. Galliano [b]

[a] *Laboratorio de Materiales Estructurales, División Cerámicos INTEMA-CONICET, Av. Juan B. Justo 4302, (7600) Mar del Plata, Argentina*
[b] *Centro de Investigación Industrial (CINI), Tenaris Siderca, Dr. Simini 250, (2804) Campana, Argentina*

Received 9 February 2008; received in revised form 22 May 2008; accepted 13 June 2008
Available online 28 August 2008

Abstract

Steelmaking electric arc furnaces (EAF) hearth is usually built up with dry vibratable refractory mixes. During furnace operation, the refractory mix undergoes sinterization, slag attack, and chemical interaction with steel. Material sintering is needed in the upper part of the EAF hearth, in order to develop enough mechanical strength and wear resistance during operation. Densification of the upper layer also reduces steel infiltration from the hot surface.

In this work, the sintering behavior of three dry vibratable commercial refractory materials for EAF hearth is reported. The characterization of the mixes includes chemical, mineralogical, and granulometric analyses. The study of sintering behavior is carried out by dilatometric analysis and microstructural and mechanical evaluation of sintered specimens.

Results showed that the analyzed mixes mainly contain periclase and doloma, with a wide granulometric distribution and different content of minor components (mainly, iron oxides). Material sintering began at temperatures higher than 1200 °C and was associated to liquid phase formation. Differences in sintering mechanisms with distinct amounts of liquid phase involved were determined in the analyzed materials and related to their iron oxides contents. Well-sintered specimens with higher room temperature mechanical strength and lower porosities were obtained from the mix with highest iron oxide content.

Keywords: Periclase–doloma refractories; Sintering; Microstructure; Mechanical properties

1. Introduction

Steelmaking electric arc furnaces (EAF) hearth is usually built up with dry vibratable refractory mixes. Their main components are usually periclase (MgO) and calcined dolomite or doloma (a mix of lime—CaO and periclase) particles[1,2] of controlled granulometric distribution and chemical purity, being iron oxide, silica and alumina the most usually found minor phases. These materials are commonly used in steelmaking refractories because their basic character, controlled manufacturing and worldwide abundance.

The performance of the EAF hearth depends on both, operative variables and materials properties. During furnace operation the refractory mix undergoes sintering, slag attack, and chemical interaction with steel. Since these phenomena occur together, it is difficult to evaluate each contribution to the in-service hearth evolution.[3,4]

Sintering of the refractory particles in the upper part of the hearth is needed in order to develop enough mechanical resistance to avoid high wear rates during campaign. Low wear of refractory hearth decreases furnace reparation frequency, refractory consumption and risk of high temperatures on the EAF metallic shell. Moreover, a high sinterability avoids steel infiltration and affects other hearth properties such as gas permeation, and thermal isolation.

The sinterability of dry vibratable mixes strongly as much as the sintering mechanism, depend on the amount and type of minor components as SiO_2, Al_2O_3 and FeO/Fe_2O_3.[5] It has been reported that especially Fe_2O_3 enhance the sintering in commercial manufacturing process of dolomite.[5]

In this work, the sintering behavior of three dry vibratable commercial mixes for EAF hearth was analyzed in relation to

* Corresponding author. Tel.: +54 223 4816600; fax: +54 223 4810046.
E-mail address: agtomba@fi.mdp.edu.ar (A.G.T. Martinez).

0955-2219/$ – see front matter © 2008 Elsevier Ltd. All rights reserved.
doi:10.1016/j.jeurceramsoc.2008.06.032

their different chemical, mineralogic and granulometric compositions in order to infer their performances in service.

2. Experimental

Three commercial dry vibratable refractory mixes (labeled A, B and C) used in steel industry for EAF hearth construction were analyzed. The refractory mixes were characterized by several techniques and their sintering behavior was studied by dilatometric and microstructural analysis together with the thermodynamic equilibrium diagrams analysis. The mechanical resistance of sintered bodies was also included in this analysis in order to achieve additional supporting information.

Granulometric analysis of as-received mixes was done by sieving between 7 (2.830 mm) and 400 (0.037 mm) mesh. A Sedigraph Micrometrics equipment was used for particle size determination under 0.037 mm. The chemical analyses of the as-received refractory mixes and of the fine granulometric fraction <0.5 mm were carried out by EDS (EDAX X-ray with a Si (Li) ultrathin window). Mineralogical analysis of both, as-received mixes and fine granulometric fractions, was done by using a Philips X'Pert powder X-ray diffractometer employing Cu Kα radiation, 40 kV, 45 mA, and a scan rate of 1.5° min^{-1}. Density of as-received refractory mixes was determined by pycnometry in kerosene at 37 °C.

Dilatometric curves were done with a dilatometer Netzsch DIL 402C using prismatic specimens formed by uniaxial pressing at 741 kg/cm^2. Tests were carried out under air or Ar up to 1600 °C at heating and cooling rates of 2 °C/min. After dilatometric analysis (1600 °C), density and porosity of the prismatic specimens were determined by weight and volume measurements and by Archimedes method in water. These samples were also ground with SiC papers up to 1200 grit for microstructural analysis. They were observed with a scanning electron microscope Philips XL30, Controlled Pressure model, with a thermoionic tungsten cathode and accelerating voltages up to 30 kV. An EDAX X-ray detecting unit with a Si (Li) ultrathin window was used for elemental analysis. $CaO–Fe_2O_3$, CaO–FeO, $MgO–Fe_2O_3$, MgO–FeO and SiO_2–CaO–FeO thermodynamic equilibrium diagrams[6] were employed for the analysis of the sintering behavior.

Fracture strength of sintered specimens was determined in diametral compression.[7] Cylinders (diameter = 30 mm; thickness = 15–17 mm) were formed by uniaxial pressing at 102 kg/cm^2 and sintered at 1400 and 1600 °C for 90 min in a rapid heating chamber electrical Lindberg/Blue BF 51664 PCOMC with $MoSi_2$ heating elements. For mechanical testing, a servo-hydraulic machine Instron 8501 with a high stiffness load frame was employed. The tests were conducted at room temperature in air, under displacement control at 0.05 mm/min, using steel compression platens.

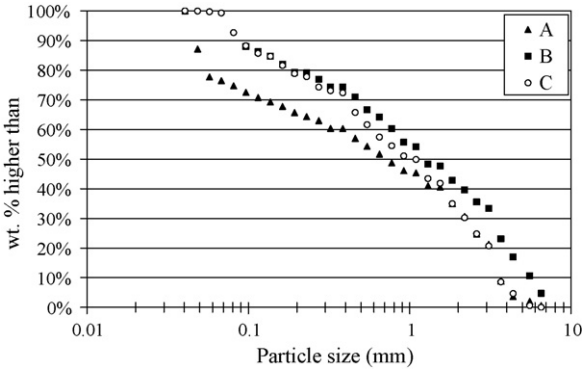

Fig. 1. Cumulative size distributions of as-received refractory mixes.

3. Results and discussion

3.1. Refractory mixes characterization

3.1.1. Granulometric analysis

Results of the granulometric analysis of A, B and C refractory mixes are displayed in Fig. 1. Every mixture showed wide granulometric distributions, between 6.00 and 0.04 mm. The parameter $W = (D_{10} - D_{90})/D_{50}$ (D_{10}, D_{90} and D_{50} are the diameters corresponding at 10, 90 and 50 wt.% of particles, respectively) was considered as a measure of the granulometric distribution width. Values of the mean particle sizes (D_{50}) and W for A, B and C refractory mixes are shown in Table 1.

As-received mix A exhibited the lowest mean particle size, the highest percentage of fine particles <0.1 mm (28 wt.%) and consequently it showed the widest granulometric distribution. The other mixes (B and C) showed granulometric distributions with similar mean particle sizes and high W values. The wide range of particle sizes determined in all granulometric distributions together with the aspect of the curves could indicate the

Table 1
Chemical and mineralogical characterization

Refractory mixes	A	B	C
Chemical analysis [wt.%][a]			
MgO	85.7–87.0	78.9–79.7	76.3–78.8
SiO_2	1.6–2.2	1–1.3	1.4–1.8
CaO	8.6–9.5	17.7–18.2	10.3–12
Fe_2O_3	1.7–1.9	0.8–1.5	7.3–8.0
MnO	0.7–1.2	0.3–0.5	–
Main crystalline phases[a]	Periclase and doloma		
Pycnometric density [g/cm^3][a]	3.43	3.44	3.50
Granulometric analysis[a]			
D_{50} [mm]	0.80	1.20	1.05
W	4.7	4.4	3.3
Chemical analysis [wt.%][b]			
MgO	85.7–87.0	90.6–92.8	77.3–79.1
SiO_2	2.3–2.6	0.9–1.6	1.5–1.8
CaO	5.3–6.5	4.0–5.0	8.3–9.1
Fe_2O_3	3.2–3.6	1.3–1.9	9.5–11.1
MnO	1.6–1.9	0.5–0.9	0.9–1.4
Main crystalline phases[b]	Periclase and doloma		
Granulometric analysis[b]			
D_{50} [mm]	0.012	0.016	–
W	2.3	1.7	–

[a] As-received.
[b] <0.5 mm.

presence of a trimodal granulometric distribution, which favors the particle packing and therefore its final densification.

Granulometric fraction <37 μm was only observed in A and B refractory mixes. In C mix, this fraction was absent. The granulometric distribution of A showed lower mean particle size and higher width than B.

3.1.2. Chemical and mineralogical analyses

Results from chemical and mineralogical characterization of A, B and C materials are shown in Table 1.

In all the as-received refractory mixes, two main crystalline phases were determined by XRD analysis: periclase[8] as the principal one and doloma[9] as the secondary phase. Periclase provides a high chemical resistance at system reacting with FeO slag to form magnesiowustite ((Mg, Fe)O) and/or with iron of the transitory liquid calcium ferrite.[6] CaO/MgO molar ratio of doloma particles analyzed by EDAX was close to unity. Taking into account XRD patterns, it was considered that Ca (Table 1) mainly arrived from doloma. According to this assumption, the doloma content estimated for refractory mixes were around 15 wt.% in A, 20 wt.% in C and 30 wt.% in B. Moreover, the obtained values of pycnometric density (3.4–3.5 g/cm^3) were in agreement with the mineralogical compositions and proportions of the phases determined in the refractory mixes.

In the fine fraction of the three granulometric distributions, similar crystalline phases were determined. A lower content of CaO with respect to the total granulometric distributions was also determined. This fact suggests that doloma level is low in particles smaller than 0.5 mm and as a consequence its granulometry is larger. Lower doloma contents in the finer particles could reduce the risk of material hydratation. The doloma contents determined in fine fractions of A and B refractory mixes were rather similar (10 and 8 wt.%) and lower than that of C (16 wt.%).

Table 2
Permanent linear change (PLC), density and porosity of sintered samples

Refractory mixes	A	B	C
PLC [%]			
1400 °C	1.6	1.8	5.85
1600 °C	3.1	3.1	11.4
Bulk density [g/cm^3]	2.84 ± 0.02	2.79 ± 0.02	3.20 ± 0.04
Apparent porosity [%]	16.50 ± 0.37	17.00 ± 0.40	2.90 ± 0.40

In addition, the iron oxide content is higher in as-received refractory mix C (>7 wt.%) than in other ones (between 0.8 and 1.9 wt.% in mixes A and B, respectively). Moreover, in all the studied refractory mixes, the iron oxide content resulted higher in the fines of the granulometric distributions (<0.5 mm). The iron oxides (Fe_2O_3/FeO) enhance the sintering ability of the material because the formation of both, a transitory liquid calcium ferrites and magnesiowustite which destabilize the periclase phase.[5]

SiO_2 and MnO were determined as others minor components (<2 wt.%) and their weight percentages resulted also slightly higher in the finer particles (<0.5 mm).

3.2. Sintering study

3.2.1. Dilatometric analysis

The curves obtained from tests carried out in air of A, B and C are shown in Fig. 2. In Table 2, PLC values at 1400 and 1600 °C for three studied refractory mixes, are shown.

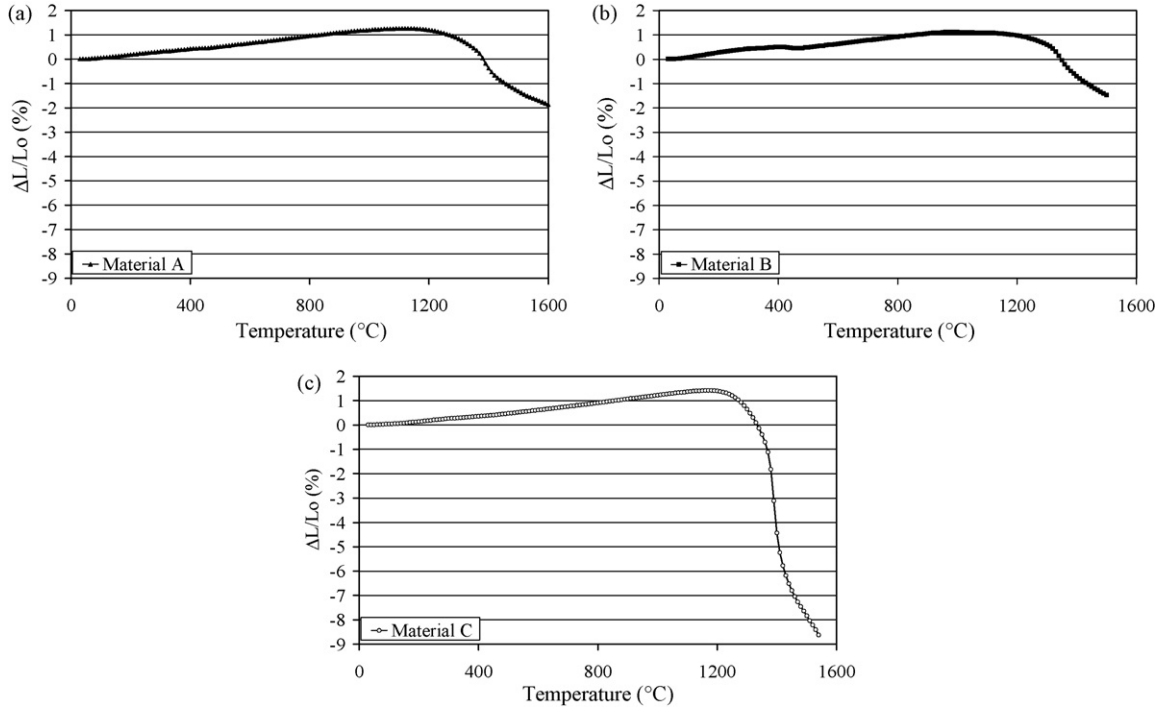

Fig. 2. Dilatometric curves for refractory mixes in air.

Non-permanent thermal expansion was observed in all materials until 1200 °C. Thermal expansion coefficient values (α) were about 10×10^{-6} °C, slightly lower than those reported for doloma ($11–13 \times 10^{-6}$ °C^{-1})[4] and MgO bricks ($13–14 \times 10^{-6}$ °C^{-1}).[3]

At temperatures between 1200 and 1300 °C, a permanent linear contraction took place in every mixes, indicating the onset of the sintering (Fig. 2). From 1300 °C, a strong increment in the densification rate of all refractory materials was registered, being most pronounced in mix C. In this material, permanent linear changes were ∼11 and ∼6% at 1400 and 1600 °C, respectively. The remaining refractory mixes (A and B) showed both, lower densification rate from 1300 °C and lower PLC values than C.

The sintering behavior exhibited by C refractory mix (large contraction and high densification rate), suggests liquid phase formation at the temperature range 1300–1600 °C, as was reported in literature.[5] Thermodynamic equilibrium diagrams[6] showed that the addition of iron oxides (FeO or Fe_2O_3) to CaO reduces its refractoriness due to liquid formation at temperatures 1100–1200 °C. This effect is less pronounced in MgO–FeO systems,[3] in which complete solid solution occurs. The formation of low melting point compounds has also been reported in literature[5] in doloma/Fe_2O_3 systems. The liquid formation in mix C at temperature >1200 °C could be attributed to the content of iron oxides and to the presence of impurities. In A and B, even when the impurity contents were similar, the amount of iron was rather lower than in C one (Table 1). In consequence, it was inferred that if liquid phase formation occurs in A and B mixes, it is in a lower degree.

Since formation temperature of liquid calcium ferrites depends on the Fe valence, dilatometric analysis in Ar atmosphere were also accomplished in order to evaluate the effect of modification in FeO/Fe_2O_3 ratio. However, no significant changes were observed between dilatometric curves in argon and in air for every mix.

3.2.2. Microstructural evolution

Bulk density and apparent porosity data of samples heated up to 1600 °C during dilatometric analysis are shown in Table 2.

Sintered bodies from A and B mixes exhibited similar porosities (16–17%), rather higher than the value obtained for material C. The lower porosity of sintered specimen obtained from C mix was an additional evidence of the higher effectiveness of the sintering mechanism in this material which, based on dilatometric curves, was previously associated to the presence of a liquid phase.

In Fig. 3 are shown SEM micrographs of the microstructures of A, B and C sintered materials after the dilatometric analysis, respectively. A liquid phase formation between the aggregates of periclase and doloma was observed in every sintered material and in the area where the liquid was located, the aggregates were rounded. The liquid phase was continuous and more abundant in this material while in A and B was present in much smaller amount. In particular, in A sintered material, the liquid phase was clearly located in triple points and in some grain boundaries and it seemed to be in a higher proportion than B. Moreover, the liquid phase was hardly to observe in the latter sample (Fig. 3b).

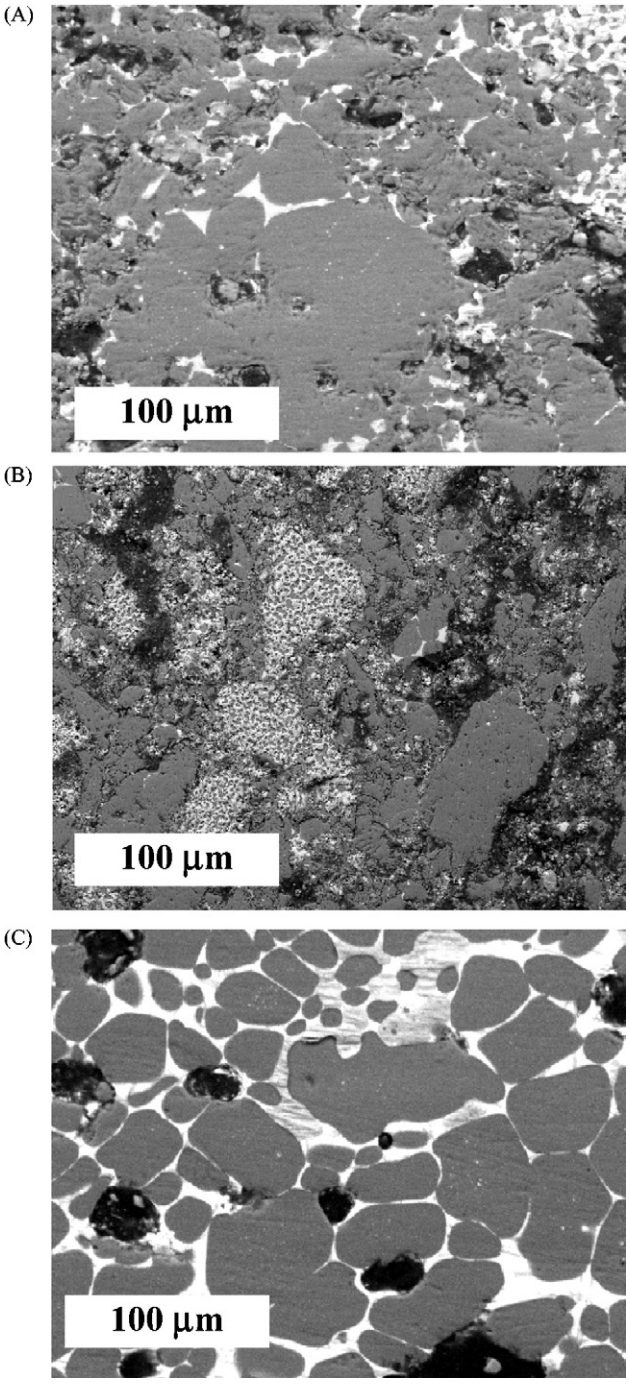

Fig. 3. Microstructure of sintered samples from refractory mixes.

The presence of a liquid during sintering of the refractory mixes, in a higher content in the Fe-rich mix (C), supports the inferences stemmed from the analysis of dilatometric curves. Furthermore, the difficult to identify the liquid in B could be related to an actual lower content of this phase (as was already inferred from dilatometric analysis) which, in turn, could be associated with the lower amount of iron oxides in as-received and fines of B mix (Table 1).

Microstructures of materials A and B exhibited higher porosity than C one, according with the their apparent porosity values (Table 2). In addition, the aspect of pores in C sintered body

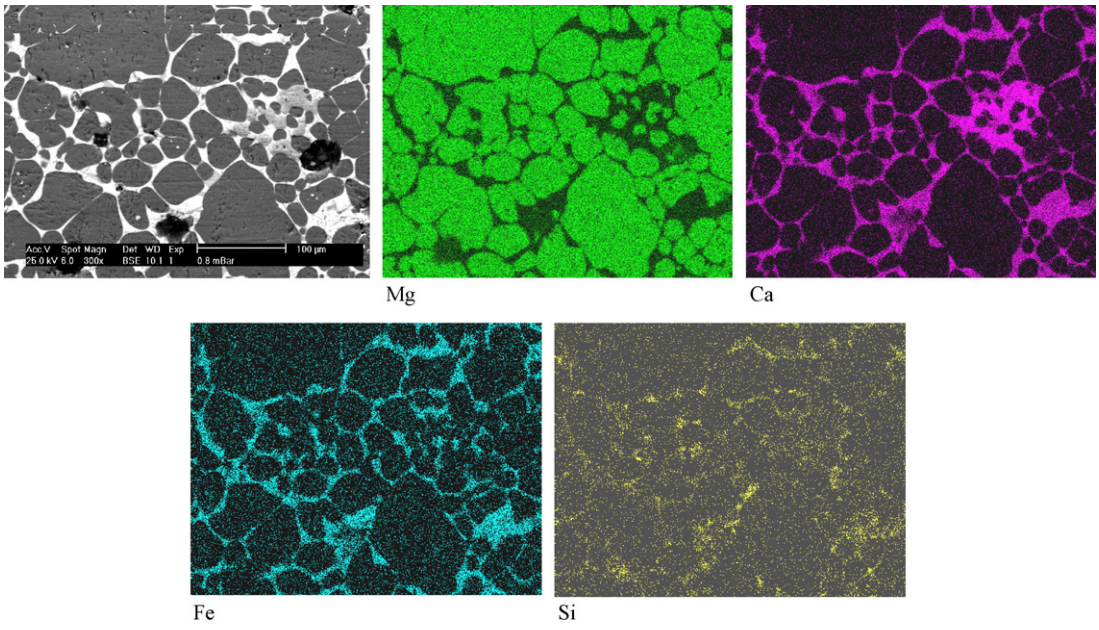

Fig. 4. Chemical microanalysis photographs of C sample.

was rather different with respect to the other two materials. Spherical isolated pores were identified around aggregates and immersed in the continuous phase in C sample. The mean pore size was similar to that of aggregates ($D_{50} \approx 0.03$ mm). In A and B sintered materials, the porosity was rather heterogeneous, with irregular pores, some of them like channels.

Solid–solid necks between particles were also observed in the microstructures of sintered samples obtained from the three mixes, which suggests that sintering effectively occurred during the thermal treatment at 1600 °C. This is also support by the contraction observed in the dilatometric curves. The formation of direct bonds was more numerous in C. From this fact, together with its high densification, a higher sintering degree could be inferred in this material.

From a global point of view, the microstructure of B sintered specimen exhibited the most marked differences with the other ones, in spite of some similarities with A. The higher amount of doloma in the as-received B mix was evident in the microstructure of the sintered material (higher content of doloma aggregates).

Chemical microanalysis showed that CaO, MgO, SiO_2 and FeO/Fe_2O_3 were the main components of the liquid phase in all materials, being more Fe-rich in C (Fig. 4).

3.2.3. Mechanical strength of sintered samples

Table 3 showed the mechanical strength values of the sintered A, B and C specimens sintered at 1400 and 1600 °C.

Table 3
Mechanical strength of A, B and C sintered specimens

Sintering temperature	Mechanical strength [MPa]		
	A	B	C
1400 °C	8.6 ± 3.0	3.8 ± 1.3	21.6 ± 0.1
1600 °C	15.5 ± 4.9	8.9 ± 1.1	19.4 ± 5.5

For sintered specimens at both temperatures (1400 and 1600 °C), mechanical strength values followed the order $C \gg A > B$. In addition, higher mechanical resistances were determined in the specimens sintered at the higher temperature, except for material C. Taking into account the standard deviation, the decrease of mean strength value of C with temperature was not considered significant. The higher mechanical resistance of C sintered specimens was consistent with its higher sintering degree (higher densification and PLC values and lower porosity) in respect of the other two materials. The difference in the strength values of A and B specimens (about 50% higher in the former) was in agreement with differences in their microstructures, in spite of the similarities in PLC and porosity values. The higher mechanical resistance of A could be indicative of a major cohesion in the material, i.e., a higher sintering degree. In a similar way, the increment of mechanical strength for A and B materials with temperature, in correlation to PLC values (Table 2), could be an indicator that the sintering degree was also increased between 1400 and 1600 °C. This behavior could be expected for any thermally activated process as sintering; due to diffusional process are involved.[10] Furthermore, an increment of the liquid content with the increasing temperature could be expected.

An independence of C's mechanical strength values, in spite of the increment in PLC values which indicates the sintering progress, was determined. If the sintering evolution implied porosity reduction and direct bond progress, the absent of a strength enhance could be attributed to the mechanical properties of the continuous phase, in addition to its changes in content, composition and distribution with the temperature increment.

3.3. Sintering mechanism

Experimental results showed that sintering began at 1200–1300 °C with liquid phase formation in every material. Nevertheless, the content of liquid was rather different

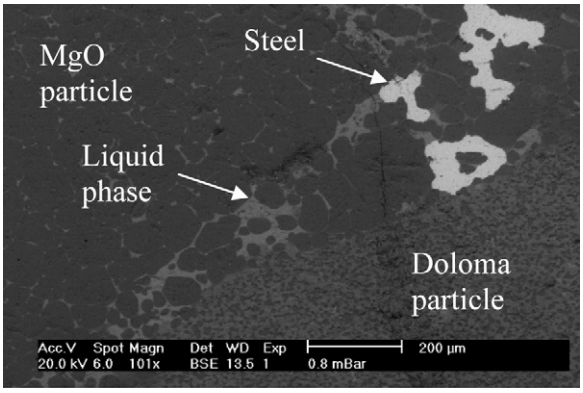

Fig. 5. Microstructure of post-mortem sample from refractory mix A. Liquid phase CaO–Fe_2O_3 rich phase (Dark grey). Steel infiltration besides the liquid phase (Bright grey).

among the refractory mixes. These facts were associated to the FeO/Fe_2O_3 content of the systems.

Microstructure of specimen C showed typical features of a liquid phase sintering mechanism[11]: high amount of liquid continuously distributed and isolated spherical pores. Moreover, a diminution of mean aggregates size was determined in C material which could be attributed to the fragmentation characteristic of the second stage of the liquid phase sintering mechanism.[11] The high PLC values and low porosity also supported this mechanism. The high amount of solid–solid necks, produced by an incipient solution–reprecipitation stage and/or solid state sintering mechanism, and the high mechanical strength were evidences of the high sintering effectiveness.

On the other hand, specimens A and B showed limited liquid and in the latter, this phase seemed to be even lower. From the microstructural characteristics together with the low PLC values and high porosities of these samples it was inferred that a small amount of liquid phase formation occurred, which limited the material transport and sintering.

The development of a liquid phase containing Ca, Mg, Si and Fe was also observed during the microstructural analysis of post-mortem refractories from EAF hearths after service (Fig. 5). It is noteworthy that even when a high amount of liquid is desirable for a rapid sintering, an excess of liquid phase could favor slag and/or steel infiltrations since the material in service interacts with liquid steel and/or slag. Thus, liquid phase control (i.e., through Fe oxide content of the refractory mix) is essential to adjust both sintering rate and sintering degree required to optimize wear resistance of the hearth material without steel infiltration risk.

4. Conclusions

The studied refractory mixes exhibited similarities in regard to the main components and the particle size distribution. However, even when the sintering began around 1200 °C in every material, the analysis of experimental data showed differences in the densification rate, the sintering degree and the mechanism involved. These facts were associated to differences in amount of liquid present at the sintering temperature which was associated to FeO/Fe_2O_3 content. The mix with the highest iron oxides content (C) showed the highest sinterability, room temperature mechanical strength, and permanent liner change, with the lowest apparent porosity. In addition, the amount of iron oxide rich liquid at the sintering temperature was higher than in the other two materials (A and B). Based on empirical evidences, a liquid phase sintering mechanism was clearly observed in mix C, while in the case of mixes A and B a smaller amount of liquid phase formation occurred, which favored materials transport and sintering up to a limited extent. A high amount of liquid phase in an iron oxide-rich mix such as C can be useful for rapid sintering (e.g. patch materials), but will also favor hearth wear due to slag and/or steel infiltration during operation.

Acknowledgement

Dilatometric analyses are gratefully acknowledged to SEGEMAR.

References

1. Verdeja, L., Parra, R., Sancho, J. and Bullon, J., Corrosion mechanism and wear prediction of the sole of an electric arc furnace. *ISIJ Int.*, 2003, **43**(2), 192–200.
2. Siegl, W., Dikalziumferritreiche Sintermagnesia in basischen Massen. *Radex-Rundschau*, 1989, **2/3**, 99–117.
3. Chesters, J. H., *Refractories—Production and Properties, Chapter 3—Magnesite*. The Iron and Steel Institute, London, 1973, pp. 118–176.
4. Chesters, J. H., *Refractories—Production and Properties, Chapter 4—Dolomite*. The Iron and Steel Institute, London, 1973, pp. 177–212.
5. Yeprem, H. A., Effect of iron oxide addition on the hydration resistance and bulk density of doloma. *J. Eur. Ceram. Soc.*, 2007, **27**, 1651–1655.
6. Acers-NIST Phase Equilibriam Diagrams, CD-ROM Database, (2004).
7. Marion, R. H. and Johnstone, J. K., A parametric study of the diametral compression test for ceramics. *Am. Ceram. Bull.*, 1977, **56**, 998–1003.
8. Freund, F., *Ber. Dtsch. Keram. Ges.*, 1970, **47**, 739.
9. Kovgan, L. N. and Nakhodnova, A. P., *Russ. J. Inorg. Chem. (Engl. Transl.)*, 1973, **18**, 208–210.
10. Kingery, W. D., Bowen, H. K. and Uhlmann, D. R., *Introduction to Ceramics (2nd ed.)*. John Wiley & Sons, 1976, pp. 469–501.
11. German, R. M., *Sintering Theory and Practice*. John Wiley & Sons, 1996 [chapter 6, pp. 225–307].